Prediction of Approximate Transition States by Bell–Evans–Polanyi Principle: I

JOSEP MARIA ANGLADA,[1] EMILI BESALÚ,[2] JOSEP MARIA BOFILL,[3] RAMON CREHUET[1]

[1]*Institut d'Investigacions Químiques i Ambientals, CID–CSIC, Barcelona, Catalunya, Spain*
[2]*Institut de Química Computacional i Departament de Química, Universitat de Girona, Campus de Montilivi, Girona, Catalunya, Spain*
[3]*Departament de Química Orgànica i Centre Especial de Recerca en Química Teòrica, Universitat de Barcelona, Martí i Franquès 1, E-08028 Barcelona, Catalunya, Spain*

Received 15 January 1999; accepted 17 March 1999

ABSTRACT: We propose a specific mathematical model of the Bell–Evans–Polanyi principle (BEP) to locate approximate transition structures of elementary reactions. The BEP adiabatic energy surface is built as a combination of three quadratic energy surfaces. Two of these quadratic energy surfaces are associated with the reactants and products, whereas the third one is associated with the crossing point energy minimum resulting from the intersection of the reactant and product quadratic energy surfaces. In this way, the resonance energy terms are taken into account. The resulting approximate transition structure and the corresponding Hessian matrix can be used as an initial geometry and a Hessian matrix to locate and optimize the true transition state on the real potential energy surface. In addition, the method provides a simple way to analyze the transition in terms of the contribution weights of the reactants and products. This model is illustrated by different numerical examples, such as the analytical Müller–Brown potential energy surface, the ring opening of cyclopropyl radical, the rearrangement of *trans*-hydroxycarbene to formaldehyde, and the rearrangement of bicyclo[3.1.0]hex-3-en-2-il radical to cyclohexadienyl radical. © 1999 John Wiley & Sons, Inc. J Comput Chem 20: 1112–1129, 1999

Keywords: transition state location; BEP principle; empirical valence-bond approach

Dedicated to the memory of Prof. M. J. S. Dewar

Correspondence to: J. M. Bofill; e-mail: jmbofill@qo.ub.es and J. M. Anglada; e-mail: anglada@qteor.cid.csic.es

Contract/grant sponsor: Generalitat de Catalunya, Spain
Contract/grant sponsor: Spanish DGICYT; contract grant numbers: PB95-0278-C02-01; PB95-0278-C02-02

CCC 0192-8651 / 99 / 111112-18

Introduction

Transition structures (TSs) determine activation energies and play key roles in reaction rate theory. A TS is located at the top of the energy barrier between reactants and products on the potential energy surface (PES). Since the formulation of transition-state theory,[1] great effort has been devoted to both locate and analyze TSs. The problem of locating TS (taken from computational quantum chemistry) is considerably more difficult than optimizing reactant and product structures (i.e., minima on the PES). The TS locating problem is inherent in the rigorous mathematical problem of defining a ''saddle point'' on a PES.[2] This mathematical definition, which is important from a computational point of view, is of little practical value in rationalizing and making predictions in regard to chemical reactivity.[3] Models are very important as a basis for design of computational algorithms and for rationalizing their results.

In the context of physical organic chemistry useful chemical models to describe TS were proposed by Bell–Evans–Polanyi (BEP),[4] Leffler,[5a] Hammond,[5b] Thornton,[5c] Marcus,[5d] More O'Ferrall,[5e] and Dewar.[5f] As pointed out by Jencks, this list is far from complete, and therefore he proposed the acronym Bema–Hapothle.[6] In its more crude form, in this model, a TS is nothing more than the minimum energy point of the intersection line defined by the PESs associated with the reactants and products. The Bema–Hapothle model enables one to define a parameter that, in some way, measures the resemblance of the TS to reactants and products on a scale from 0 to 1. According to this, a TS is a hybrid of the reactant and product structures and, consequently, its behavior is intermediate, or an average of reactant and product behavior. As Salem[7] pointed out, in this model, the potential surface along the reaction coordinate is approximated by a linear combination of two harmonic potentials associated with the reactants and products; that is, the PESs of the reactants and products are expanded quadratically around the stationary points associated with the corresponding equilibrium geometries. The TS occurs at the intersection minima of the two parabolas. This is in fact the diabatic surface model of TSs based on the intersection of two surfaces.[4h, i, 8a–d] These ideas can be expressed mathematically using the following Lagrangian function:

$$L(\mathbf{q}, \lambda) = w_R V_{RR}(\mathbf{q}) + w_P V_{PP}(\mathbf{q}) + \lambda(V_{RR}(\mathbf{q}) - V_{PP}(\mathbf{q})) \quad (1a)$$

$$V_{RR}(\mathbf{q}) - V_{PP}(\mathbf{q}) = 0 \quad (1b)$$

where $\mathbf{q}$ are the internal coordinates describing a reaction path leading from reactants to products; V_{RR} and V_{PP} are the PESs for reactants and products, respectively, which are assumed to be harmonic; λ is a Lagrangian multiplier; and, finally, w_R and w_P are two weights such that $w_R + w_P = 1$. However, other developments relating the TS to reactants, products, and intermediates have also been proposed.[5c, e]

Based on eqs. (1), many algorithms exist to locate TSs in an approximated way. To our knowledge, the first algorithm was given by Robb et al.[9] In their algorithm, the two diabatic surfaces, V_{RR} and V_{PP}, are not restricted to be quadratic around the equilibrium geometry and $w_R = 1$. From a computational point of view, the algorithm implementation is based on the Lagrange–Newton minimization crossing point between two surfaces as proposed by Morokuma et al.[10] Using the same philosophy, other investigators have proposed slightly different models. Jensen[11] proposed a model in which the two intersecting surfaces associated with reactants and products are evaluated using a force field rather than quantum mechanically. Finally, Ruedenberg and Sun[12] proposed a very elegant algorithm in which the two diabatic surfaces, V_{RR} and V_{PP}, associated with the reactants and products, are modeled as quadratic expansions around its equilibrium geometries and $w_R = w_P = 1/2$. In this way, the approximated point for the TS is the minimum point of the intersection line defined by the two quadratic PESs of reactants and products as the Bema–Hapothle principle requires. From a computational point of view, in the Ruedenberg and Sun[12] algorithm, the multidimensional problem for finding the stationary point of eqs. (1) is reduced to find the zero point of a one-dimensional nonlinear function.

As pointed out by Jensen,[11b] in all of the preceding crude models to describe TSs, the quantum mechanical resonance is neglected. Consequently, because the geometry of the minimum crossing point of the intersection between the two PESs is equated to be the best approximate geometry of the real TS then the PES near the TS presents a

discontinuity.[11b] In addition, the effect of neglecting the resonance integral is that the approximate TS geometry is a hybrid of the reactant and product structures. This hybrid TS sometimes presents an unbalanced or inappropriate bond break–bond formation. In this situation, the resonance effects should be introduced in some way to give a better approximate TS geometry.

Due to this drawback, Pross and Shaik[13] proposed an alternative model to TS based on Evans's ideas[4h] of curve crossing. In their model the TS is located in a region of avoided crossing (AC) of the Heitler–London (HL) valence bond (VB) configuration wave function that describes the bonding of reactants and products. However, Pross and Shaik[13] enable mixing of other VB configurations, so-called ''intermediate configurations,'' which are important only in the TS region, with the HL configurations. The resulting wave function gives a more complete description of the TS region. Mathematically, this is expressed as:

$$\Psi_{TS} \cong \Psi_{ACS} = (1 + \mu^2)^{-1/2} \times \{2^{-1/2}[\Phi_R(HL) + \Phi_P(HL)] + \mu\Phi_I\} \quad (2)$$

where Ψ_{ACS} is the avoided crossing state wave function and μ is the mixing coefficient of the intermediate configuration. Using this model, the normal procedure to locate and analyze a TS consists of: (1) writing the wave function of reactants and products as a linear combination of VB configurations related to the classical Lewis structures, that is, Φ_R(HL) and Φ_P(HL); (2) locating the surface crossing point of these two VB wave functions; and (3) at this point, the intermediate configurations, Φ_I, are included by performing a variational calculation. Finally, the resonance integral is evaluated as a difference between the TS and crossing point energies. These ideas have been applied using *ab initio* VB wave functions in reaction systems in which the surface crossing point and, consequently, the TS, is determined by the symmetry of the reaction, such as S_N2 reactions type $X^- + RX$. This model also enables one to describe the S_N2 reaction systems as one-dimensional systems by making some assumptions about the reaction coordinate such as the conservation of bond order.[11a, 14]

Finally, we mention the work of Warshel,[15] who proposed the so-called empirical valence bond (EVB) approach for comparing PESs of reactions in solution. The EVB approach can be seen as a mathematical model of the BEP principle in which the resonance effects are taken into account in some empirical way.[15a] More recently, using the same philosophy, Kim and Hynes[16] proposed a TS structure model for the S_N1 ionic dissociation in solution.

In the present study, we propose a method based on a specific modeling of the BEP principle that gives approximate TS structures in an inexpensive way. In addition, the method generates a Hessian matrix that can be used as the starting Hessian matrix needed to optimize the TS structure using standard Newton–Raphson (NR) methods.[2, 17] Also, we use the proposed BEP method to analyze the TS structure. This study is organized as follows: first, we present the mathematical basis and the implementation algorithm of the proposed BEP model that takes into account the resonance effects; and, second, we illustrate the method by application to TS on analytical, semiempirical, and *ab initio* PESs.

Theoretical Basis and Algorithm Implementation

MATHEMATICAL BACKGROUND

In the BEP method one can see the PES model as a result of quantum chemical calculation with a two-state electronic wave function:

$$\Psi_{PES} = c_R\Phi_R + c_P\Phi_P \quad (3)$$

where Φ_R is the wave function that describes the electronic structure of the reactants and Φ_P the wave function that describes the electronic structure of the products. The ground state Born–Oppenheimer PES (i.e., the adiabatic PES) corresponds to the lower root of a 2×2 secular equation, V_{adi}, given by:

$$V_{adi} = \frac{V_{RR} + V_{PP}}{2} - \left[\left(\frac{V_{RR} - V_{PP}}{2}\right)^2 + V_{RP}^2\right]^{1/2} \quad (4)$$

where $V_{RR} = \langle\Phi_R|H_{ele}|\Phi_R\rangle$, $V_{PP} = \langle\Phi_P|H_{ele}|\Phi_P\rangle$, $V_{RP} = V_{PR} = \langle\Phi_R|H_{ele}|\Phi_P\rangle$, and H_{ele} is the electronic Hamiltonian that depends on the nuclear coordinates. Consequently, V_{RR}, V_{PP}, V_{RP}, and V_{adi} also depend on the nuclear coordinates. To connect the BEP model with the Pross and Shaik model we need to change the Ψ_{PES} given in eq. (3) by:

$$\Psi_{PES} = c_R\Phi_R + c_P\Phi_P + c_I\Phi_I \quad (5)$$

where Φ_I represents a set of intermediate (typical ionic) configurations. Using the wave function of eq. (5), one obtains a 3×3 secular equation. However, according to Löwdin's partitioning technique[18] we again recast a 2×2 secular equation as required by the BEP model (see Appendix A1).

In the present model, elements V_{RR}, V_{PP}, and V_{RP} are not calculated according equations (A1-6). Thus, in the BEP model, V_{RR} and V_{PP} are related to the diabatic PESs associated with the single minimum region that describes the nonreactive motion of the reactants and products, respectively. The local harmonic approximation or quadratic approximation around the equilibrium geometry of reactants and products is the simplest model for both V_{RR} and V_{PP}, respectively. The important and crucial part of the BEP model is the resonance matrix element, V_{RP}, of which is not obvious as to how it should be approximated. In this study, we employ the Chang and Miller[19] approximation, which has been employed several times for other purposes.[20] The corresponding mathematical expressions are given in Appendix A2, although there are other possibilities, such as the one given by Warshel.[15] Warshel's group selected a V_{RP} in such a way that the BEP potential model, V_{adi}, given by eq. (4), reproduces exactly the local harmonic approximation or quadratic approximation of the real PES around the TS, $\mathbf{q}_{TS}$.

Substituting eqs. (A2-3) and (A2-7) in eq. (4) we obtain an expression for the BEP adiabatic PES, V_{adi}. Because we are interested in the location and geometry optimization of the TS in the BEP adiabatic PES, in Appendix A3 we give the corresponding gradient and Hessian expression of V_{adi} in internal coordinates, $\mathbf{q}$. These expressions were derived for the first time in a more general form by Minichino and Voth.[20]

COMPUTATIONAL DETAILS

Using the results of the preceding subsection we are almost ready to employ any type of NR algorithm to optimize TS geometry in the proposed BEP adiabatic PES, V_{adi}, as the so-called restricted quasi-Newton–Raphson/rational function optimization or augmented Hessian algorithm (RQNR/RFO).[21] At this point, two questions arise: (1) What is the geometry of $\mathbf{q}_0$ and its corresponding V^0_{adi}, $\mathbf{g}^0_{adi}$, and $\mathbf{H}^0_{adi}$ that are needed to define V_{adi} according to the equations defined in Appendix A2 and eq. (4)? (2) What is the starting geometry, $\mathbf{q}^0_{TS}$, that any RQNR/RFO algorithm needs to start the optimization in the V_{adi}? A solution to both questions consists of taking $\mathbf{q}_0 = \mathbf{q}^0_{TS} = \mathbf{q}_{CP}$, where $\mathbf{q}_{CP}$ is the solution of Lagrange eqs. (1) taking V_{RR} and V_{PP} as defined in eq. (A2-5), which uses the harmonic approximation. Some comments are needed with respect to V^0_{adi}, $\mathbf{g}^0_{adi}$, and $\mathbf{H}^0_{adi}$. The value assigned to V^0_{adi} is that of the real PES at $\mathbf{q}_{CP}$. On the other hand, for the selection and evaluation of $\mathbf{g}^0_{adi}$ and $\mathbf{H}^0_{adi}$ two strategies exist. The first one consists of equating $\mathbf{g}^0_{adi}$ and $\mathbf{H}^0_{adi}$ to the gradient vector and Hessian matrix of the real PES at $\mathbf{q}_{CP}$. The second is to take that gradient vector and Hessian matrix as just the gradient and the Hessian of the objective function of eq. (1); that is, $w_R V_{RR} + w_P V_{PP}$ at $\mathbf{q}_{CP}$. In the last option the spectra of the Hessian matrix should be modified adequately. This fact is explained in what follows.

Using the aforementioned ideas, we describe a step procedure that finds the TS of the proposed BEP adiabatic PES model:

1. Given $\mathbf{q}_R$, V^*_{RR}, $\mathbf{H}_R$, $\mathbf{q}_P$, V^*_{PP}, and $\mathbf{H}_P$, find the minimum energy crossing point, $\mathbf{q}_{CP}$, of the intersection of the two quadratic PESs, V_{RR} and V_{PP}. In other words, solve eq. (1) taking V_{RR} and V_{PP} as given in eq. (A2-5). This can be done very efficiently using the algorithm described by Ruedenberg and Sun.[12] Because the minimum energy crossing point, $\mathbf{q}_{CP}$, is invariant under variations of the weights w_R and w_P, one can take any value within the condition $w_R + w_P = 1$. However, as we will see, we take the value $w_R = w_P = 1/2$. Note that the Lagrangian multiplier, λ, introduced in eq. (1), is restricted to satisfy the inequality $-w_R < \lambda < w_P$ (see Appendix A4).
2. Compute the value of the real PES at $\mathbf{q}_{CP}$ and take this as V^0_{adi}. In this way, we are able to introduce the intermediate configurations, Φ_I, as proposed by Pross and Shaik.[3, 13b]
3. This step can be carried out in two different ways namely, options 3A and 3B, depending on the difficulty of computing the gradient vector and Hessian matrix of the real PES. If the gradient and Hessian matrix are easy to evaluate then we use:

   - *Option 3A*. Compute the gradient vector and the Hessian matrix of the real PES at $\mathbf{q}_{CP}$ and take these as $\mathbf{g}^0_{adi}$ and $\mathbf{H}^0_{adi}$. Make sure that $\mathbf{H}^0_{adi}$ possesses the desired spectra. This is done by forcing all eigenvalues to be positive except the eigenvalue

associated with the eigenvector that is the potential transition vector.

Otherwise:

- *Option* 3*B*. The gradient vector, $\mathbf{g}^0_{adi}$, is approximated as $w_R\mathbf{g}_R + w_P\mathbf{g}_P$, where $\mathbf{g}_R$ and $\mathbf{g}_P$ are the gradient vectors of the quadratic potentials V_{RR} and V_{PP} at $\mathbf{q}_{CP}$, respectively, and the Hessian matrix $\mathbf{H}^0_{adi}$ as $w_R\mathbf{H}_R + w_P\mathbf{H}_P$. Because both $\mathbf{H}_R$ and $\mathbf{H}_P$ matrices are positive definite, the resulting Hessian matrix does not possess the correct spectra, so it is changed in the following way. At point $\mathbf{q}_{CP}$, the vector $N(\mathbf{g}_R - \mathbf{g}_P)$, where N is a normalization factor, is a vector that is perpendicular to the seam defined by the intersection of the two quadratic surfaces V_{RR} and V_{PP}. Consequently, the topological structure of this vector should be close to the desired transition vector. Selecting the eigenvector of the $\mathbf{H}^0_{adi}$ that more resembles the vector $N(\mathbf{g}_R - \mathbf{g}_P)$ and forcing its eigenvalue to be negative and all the remaining eigenvalues to be positive, we already have a $\mathbf{H}^0_{adi}$ matrix with the desired spectra. In the present work, the weights, w_R and w_P, are taken to be $w_R = w_P = 1/2$. However, other selections are possible by considering the Hammond postulate;[5b] in this case, the weights should be computed via the Marcus equation.[5d] If we consider the situation in which the weights are $w_R = w_P = 1/2$ and taking into account the fact that, at the $\mathbf{q}_{CP}$, $V^0_{RR} = V^0_{PP}$, and then $\mathbf{b}_0$ vector is equal to the zero vector and the $\mathbf{B}_0$ matrix takes the following form:

$$\mathbf{B}_0 = \frac{1}{V^0_{RR} - V^0_{adi}}(\mathbf{H}_R + \mathbf{H}_P - 2\mathbf{H}^0_{adi}) - \frac{1}{2}\frac{1}{(V^0_{RR} - V^0_{adi})^2} \times (\mathbf{g}^0_R - \mathbf{g}^0_P)(\mathbf{g}^0_R - \mathbf{g}^0_P)^T \quad (6)$$

Consequently, the square of the resonance energy matrix term given in eq. (A2-7) is reduced to:

$$V^2_{RP} = A_0 \exp\left(\tfrac{1}{2}\Delta\mathbf{q}_0^T\mathbf{B}_0\Delta\mathbf{q}_0\right) \quad (7)$$

4. Using eqs. (4), (A3-1), and (A3-3), coupled in an iterative NR algorithm type to locate saddle points,[21] find the TS predicted by the BEP principle mathematically modeled as described in what follows. Specifically, we used the algorithm described in reference 21k. The initial geometry $\mathbf{q}^0_{TS}$ and Hessian matrix that this type of algorithm need are those corresponding to the minimum energy crossing point, $\mathbf{q}_{CP}$, obtained as described in eq. (3). Also, this crossing point is the $\mathbf{q}_0$ point where the A_0 scalar, $\mathbf{b}_0$ vector, and $\mathbf{B}_0$ matrix are evaluated, as given in eqs. (A2-8), (A2-9), and (A2-10), respectively. To achieve good efficiency during the iterative process parameters A_0, $\mathbf{b}_0$, and $\mathbf{B}_0$ are evaluated at each iteration rather than kept constant. That is, the optimal point of an iteration and the current BEP adiabatic energy, gradient, and Hessian matrix are used to evaluate the new parameters A_0, $\mathbf{b}_0$, and $\mathbf{B}_0$ for the next iteration. Finally, we say that the current Hessian matrix at each iteration can be updated using standard formulas[17] rather than evaluated analytically using eq. (A3-3).

Because it is assumed that the quadratic energy expansion around $\mathbf{q}_{CP}$, V^0_{adi}, possesses a stationary point, the real TS point, $\mathbf{q}_{TS}$ (see Appendix A2), the aforementioned algorithm has a weak point. In fact, this is the main assumption of the BEP principle,[4,7] that is the $\mathbf{q}_{CP}$ point is close to the $\mathbf{q}_{TS}$ point and this should be true in many cases because this principle satisfactorily explains the chemical reactions.[5,6,13] If the Hessian matrix at point $\mathbf{q}_{CP}$ presents more than one negative eigenvalue, then this quadratic energy expansion does not contain the $\mathbf{q}_{TS}$ point. In this situation one should modify the Hessian matrix such that it possesses the desired spectra, and that it forces all eigenvalues to be positive except the eigenvalue associated with the potential transition vector. Finally, from a computational point of view, the present algorithm is inexpensive except for step 2 and option 3A of step 3. Option 3B of step 3 needs some clarification. First, this option should be used very carefully. A necessary but not sufficient criterion to be considered to determine whether this option can be used consists of regarding the largest value of all the square overlaps between the vector $N(\mathbf{g}_R - \mathbf{g}_P)$ and the set of eigenvectors $\{\mathbf{v}_i\}_{i=1}^n$ of the matrix $w_R\mathbf{H}_R + w_P\mathbf{H}_P$:

$$s = \max\left\{\left[\mathbf{v}_i^T\left(N(\mathbf{g}^0_R - \mathbf{g}^0_P)\right)\right]^2,\ i = 1, \ldots, n\right\} \quad (8)$$

Note that the s scalar is defined within the interval $0 < s \leq 1$. If the s parameter is small, say lower than 0.5, then option 3B should not be used; otherwise, if the resonance effects are weak or if they are strong but only in the direction of the vector $N(\mathbf{g}_R - \mathbf{g}_P)$ then the algorithm will converge to a TS geometry that will be reasonably close to the real TS geometry. The converged TS geometry takes into account the resonance effects and, consequently, is much closer to the real TS geometry than the minimum energy crossing point, $\mathbf{q}_{CP}$, geometry. However, it is important to emphasize that option 3A should be used in general rather than option 3B, because the latter option assumes a set of strong approximations. Option 3B should be employed only in cases in which the gradient vector and Hessian matrices are very expensive to compute.

We conclude that, using the above algorithm, the TS geometry found and the corresponding Hessian matrix evaluated according to eq. (A3-3) are both good initial geometry and Hessian to start the optimization of TS geometry on the real PES using the NR-type algorithm.[2]

Numerical Results and Examples

ANALYTICAL SURFACE OF MÜLLER–BROWN

We employed the analytical PES proposed by Müller–Brown,[22] defined in Appendix A5, to study the performance of the present method. The coordinates are in angstroms and the energy in millihartree. The PES has three minima, M1, M2, and M3, and two TSs, TS1 and TS2. TS1 connects M1 and M2, and TS2 connects M2 and M3. Consequently, the Müller–Brown analytical PES[22] can be seen as a representation of a potential surface associated with a reaction that occurs in two steps through the intermediate M2. The calculations and graphic representations were carried out using the MATHEMATICA program.[23] Table I gives the coordinates, energies, and Hessian matrices of the five stationary points, M1, M2, M3, TS1, and TS2.

Figure 1 shows the results of the study of the first elementary reaction that involves the M1 and M2 minima obtained by applying the aforementioned algorithm. The red lines are the real Müller–Brown surface and the blue lines are the BEP model surface for this elementary reaction. The CP1 point is the minimum energy crossing point between the two quadratic surfaces centered in minima M1 and M2 associated with the reactant and product of this elementary reaction, previously reported by Ruedenberg and Sun.[12] The point TS1 is the real transition state, whereas TSa1 corresponds to the optimized transition state of the BEP model surface. Table II shows the energy, gradient, and Hessian matrix of CP1 and TSa1, evaluated on the Müller–Brown PES. Comparing the geometry parameters of CP1 and TSa1 with those of TS1, we observe that TSa1 is much closer to TS1 than CP1. The energy differences of CP1 and TSa1 with respect to TS1 are −16.79 mH and 1.19 mH, respectively. The small energy difference between TSa1 and TS1 is reflected in the small value of the gradient components, corroborating that TSa1 is very close to be the real stationary point. Proceeding as before, Figure 2 shows the behavior of the proposed algorithm in the study of the second elementary reaction associated with minima M2 and M3. Based on Figure 2, the position of both points, TS2 and TSa2, and their coordinates in Tables I and II, respectively, we conclude that the BEP surface model predicts the exact transition structure for this elementary reaction within a very small error. This is reflected in the gradient components of TSa2 shown in Table II. The CP2 point that is the minimum energy crossing point between the two quadratic surfaces centered in the M2 and M3 minima is −4.05 mH below TS2. In Table II, we note that CP2 possesses large gradient

TABLE I.
Coordinates, Energies, and Hessian Matrices of the Five Stationary Points M1, M2, M3, TS1, and TS2 of the Müller–Brown Potential Energy Surface.

	x (Å)	y (Å)	E (mH)	H_{xx}	H_{xy}	H_{yy}
M1	−0.5582	−1.4417	−146.70	2241.1	−1828.8	2237.6
M2	−0.0500	0.4667	−80.77	239.6	151.6	1460.6
M3	0.6235	0.0280	−108.17	553.6	154.9	2995.6
TS1	−0.8220	0.6243	−40.66	−229.3	612.6	−31.3
TS2	0.2125	0.2929	−72.25	198.9	539.9	−423.7

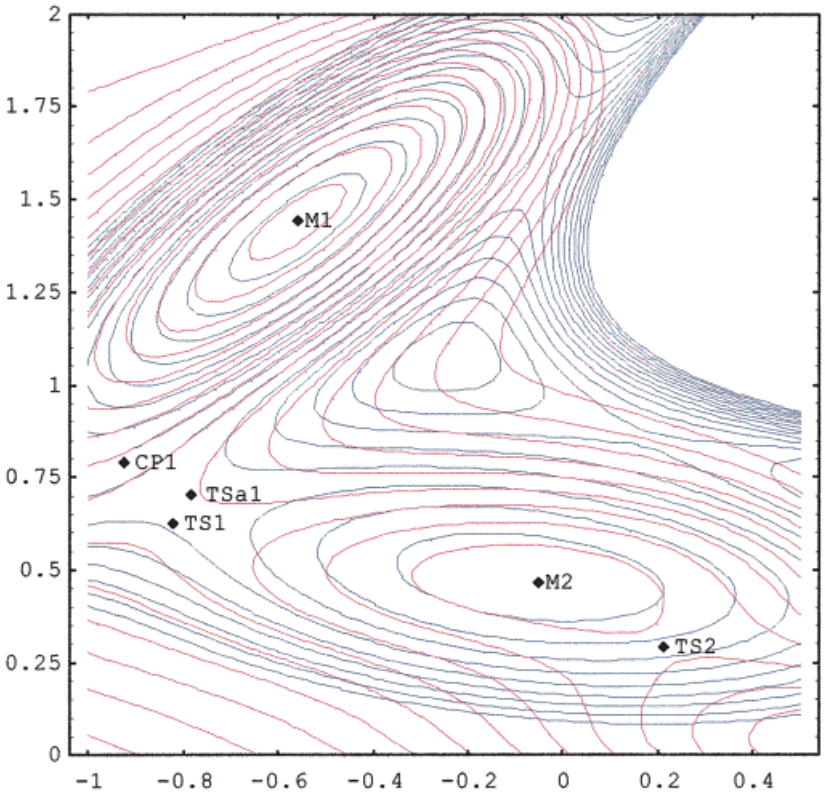

FIGURE 1. Müller–Brown potential energy surface (PES) for the first elementary reaction (see text). Red lines represent the real Müller–Brown PES, and the blue lines represent the BEP PES model. In both cases, the contour lines correspond to an energy increment of 11.3 mH. Minima: M1, M2; crossing point: CP1; real transition state: TS1; transition state of the BEP PES model: TSa1.

components. This point was previously reported by Ruedenberg and Sun.[12]

Figures 3 and 4 show the difference, in absolute value, between the Müller–Brown and the corresponding BEP model PESs, denoted V and V_{adi}, respectively, for the two elementary reactions. Regarding both figures, we conclude that, in the more relevant region of the real PES, $|V - V_{adi}|$ is less than 1.0 mH. Considering the relative simplicity of the proposed BEP model surface, we conclude that it represents the Müller–Brown PES very well. Consequently, it can be used to locate, with very good approximation, the TSs.

As pointed out by Ruedenberg and Sun,[12] the TS1 stationary point is very difficult to locate. Looking at Figure 3, the CP1 is close to TS1; however, its associated quadratic region still does not contain TS1. The composition of vector $(N(\mathbf{g}_1 - \mathbf{g}_2))^T$ at CP1 is (0.428, −0.904) and the transition vector of TS1 is (0.761, −0.649). On the other hand,

TABLE II.
Coordinates, Energies, Gradients, and Hessian Matrices of Crossing Points between Corresponding Quadratic Surfaces (CP1 and CP2) and Approximate Transition States Predicted by BEP Method (TSa1 and TSa2) for Müller–Brown Potential Energy Surface.

	x (Å)	y (Å)	E (mH)	g_x	g_y	H_{xx}	H_{xy}	H_{yy}
CP1	−0.9231	0.7887	−57.45	91.606	−146.048	408.6	188.9	−665.9
CP2	0.3518	0.2302	−76.30	−7.725	114.225	239.6	633.2	−417.0
TSa1	−0.7820	0.7022	−39.47	43.696	2.272	−246.4	742.8	−622.1
TSa2	0.2153	0.2937	−72.25	0.958	1.175	200.4	540.7	−423.1

at CP1, the Hessian matrix possesses a negative eigenvalue with the eigenvector (0.168, −0.986). Clearly, we observe that the quadratic surface around CP1 still presents some differences with respect to the quadratic surface around TS1. At the converged point TSa1, the Hessian matrix evaluated according to eq. (A3.3) shows a negative eigenvalue with the eigenvector (0.830, −0.557), which resembles the real transition vector. Even in this situation the present method is powerful enough to give a point, TSa1, that is very close to TS1 in terms of both geometry and Hessian matrix. It is also of interest to see that the scalar s, defined in eq. (8) for this elementary reaction, is 0.97; however, because the vector $N(\mathbf{g}_1 - \mathbf{g}_2)$ differs from the real transition vector, we note that use of option 3B does not permit adequate convergence at the desired saddle point. This is an example in which scalar s is a necessary but insufficient criterion to determine if option 3B should be used or not.

For the second elementary reaction the three vectors, namely $(N(\mathbf{g}_2 - \mathbf{g}_3))^T$, the transition vector of TS2, and the eigenvector of the lowest eigenvalue of the Hessian matrix at CP2, are (0.207, −0.978), (0.500, −0.865), and (0.520, −0.854), respectively. Clearly, the quadratic expansion around CP2 contains TS2. This is the reason way TSa2 is very close to the real transition state. The Hessian matrix evaluated according to equation (A3-3) at TSa2 shows a negative eigenvalue with the eigenvector (0.515, −0.857), which is almost the real transition vector. The scalar s, defined in eq. (8) for this elementary reaction, is 0.92. Therefore, option 3B can be used to locate TS2. Note that, in this example, both the $(N(\mathbf{g}_2 - \mathbf{g}_3))^T$ vector and the transition vector have the same topology.

CYCLOPROPYL RADICAL RING OPENING

The thermal conversion of cyclopropyl radical (CR) into allyl radical (AR) was studied theoretically at the semiempirical and *ab initio* levels of theory by Olivella et al.[24] One of the main conclusions of this study is that, in spite of the symmetry of both the reactant and product, this electrocyclic

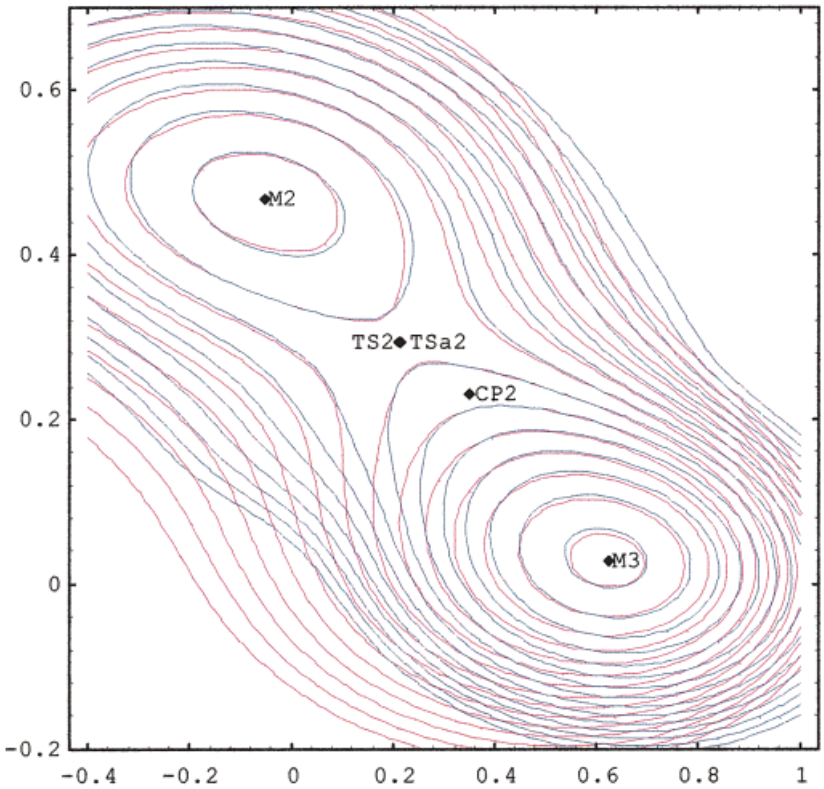

FIGURE 2. The Müller–Brown potential energy surface (PES) for the second elementary reaction (see text). Red lines represent the real Müller–Brown PES, and the blue lines represent the BEP PES model. In both cases, the contour lines correspond to an energy increment of 5.3 mH. Minima: M2, M3; crossing point: CP2; real transition state: TS2; transition state of the BEP PES model: TSa2.

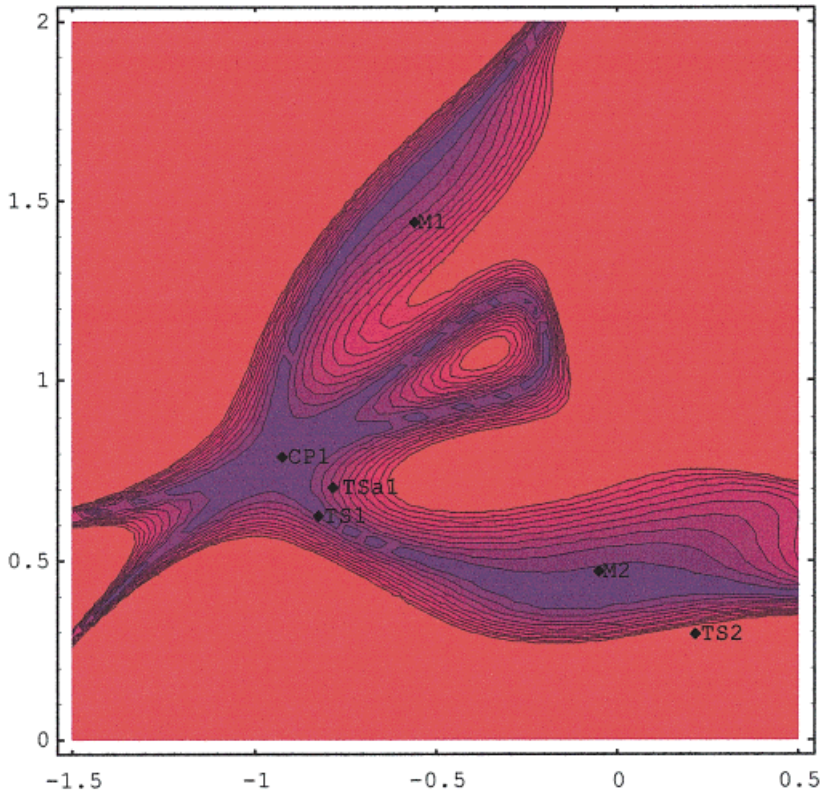

FIGURE 3. The difference in absolute value between the Müller–Brown potential energy surface (PES) and the BEP PES model for the first elementary reaction (see text). The contour lines correspond to an energy increment of 1.0 mH. In the blue region, $|V - V_{adi}| \leq 1.0$ mH; in the red region, $|V - V_{adi}| \geq 10.0$ mH. Minima: M1, M2; crossing point: CP1; real transition state: TS1; transition state of the BEP PES model: TSa1.

reaction takes place through a highly nonsymmetric TS. The thermal interconversion between CR and AR is both orbital and state symmetry forbidden, regardless of mode (conrotatory or disrotatory) of methylene group considered. The question remains as to how good the described BEP model is in giving an approximate TS structure for this reaction. We studied this reaction using the AM1 semiempirical Hamiltonian[25] and the UHF wave function. It has been pointed out that the UHF wave function is appropriate for studying this reaction.[24] The AM1 Hamiltonian was chosen because it predicts erroneously that the equilibrium geometry of CR has C_{2v} symmetry, rather than C_s. This is the more unfavorable situation for prediction of nonsymmetric TS because both reactant and product have C_{2v} symmetry.

The dihedral angles of the hydrogen atoms of the two methylene groups of CR and AR are related through a conrotatory reaction path. Because both conrotatory and disrotatory reaction paths are forbidden,[24] here we present only the results for the conrotatory reaction path. The geometry of the minimum energy crossing point, CP, of the intersection between the two quadratic surfaces centered in CR and AR has C_2 symmetry, which is the symmetry of the conrotatory motion. We carried out calculation of the energy, gradient, and Hessian matrix at CP on the real UHF/AM1 PES, following steps 2 and 3A of the algorithm given earlier. The CP on the UHF/AM1 PES lies 36.5 kcal mol^{-1} above the minimum CR. The Hessian matrix at CP possesses two negative eigenvalues, one corresponds to the symmetric motion and the other to the breaking symmetry motion. The geometries, energies, gradients, and Hessian matrices of CR, AR, and CP define the quadratic expansions needed to build the BEP surface model as discussed earlier. Starting at CP, saddle point optimization is carried out on this BEP surface model. During the optimization process the Hessian matrix is forced to have a negative eigenvalue. The negative eigenvalue corresponds to the eigenvector, which breaks the symmetry.

The optimization process found a point of C_1 symmetry, denoted TSa, with a gradient norm of

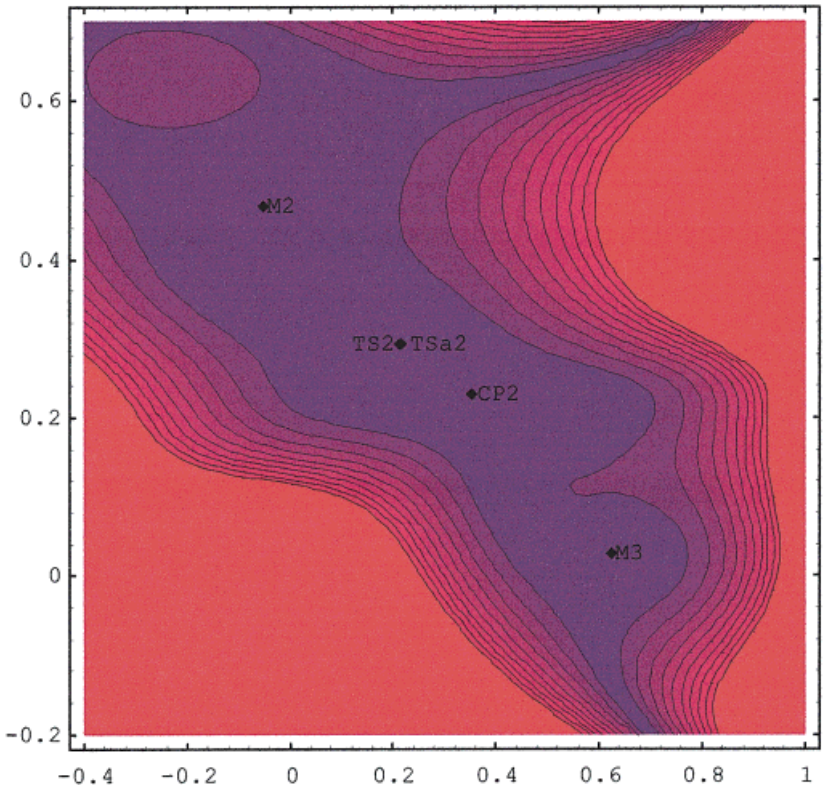

FIGURE 4. The difference in absolute value between the Müller–Brown potential energy surface (PES) and the BEP PES model for the second elementary reaction (see text). The contour lines correspond to an energy increment of 1.0 mH. In the blue region, $|V - V_{adi}| \leq 1.0$ mH; in the red region, $|V - V_{adi}| \geq 10.0$ mH. Minima: M2, M3; crossing point: CP2; real transition state: TS2; transition state of the BEP PES model: TSa2.

0.11 kcal/mol $Å^{-1}$. Diagonalizing the Hessian matrix of TSa, computed according to eq. (A3-3), it was found that TSa is the transition state predicted by the proposed BEP model. The geometries of CR, AR, CP, TSa, and the true TS of the UHF/AM1 PES are displayed in Table III. To assess the proximity of both CP and TSa geometries with respect to the true TS we introduce the root-mean-square distance (RMS; in angstroms) and radians between these points. The RMS (CP − TS) = 0.88, while the RMS (TSa − TS) = 1.12; consequently, CP is much closer to TS than TSa. However, because CP possesses C_s symmetry, if one takes this as the starting point for any NR algorithm for locating the true saddle point the algorithm does not converge. On the other hand, TSa possesses the same symmetry as TS. Taking this point as the starting point for the NR algorithm, it converges to the real TS. In other words, despite CP being much closer to TS than TSa, TSa is a better starting point for any NR algorithm for locating saddle points when compared with CP.

This example reveals the importance of including the resonance energy term in the study of TSs, as Pross and Shaik noted.[13] The CP can be seen as a natural hybrid of CR and AR and, consequently, the geometry differences between CP and TSa are due solely to the inclusion of the resonance energy. The present BEP model indicates that the resonance term plays an important role in this electrocylic reaction. To give numerical support to this affirmation, we note that the values of element $V_{CR,AR}$ of the matrix equation (A1-5) at $\mathbf{q}_{CP}$ and $\mathbf{q}_{TSa}$, evaluated as the square root of eq. (A2-7), are -20.6 kcal mol^{-1} and -71.2 kcal mol^{-1}, respectively.

The BEP model enables quantitative analysis of the contribution of reactants and products for the description of the TSa structure. The two weights are evaluated as the square of coefficients c_R and c_P in eq. (A1-5), computed at TSa. In the present case, we have $(c_{CR})^2 = 0.52$ and $(c_{AR})^2 = 0.48$ and we conclude that CR and AR contribute equally to the description of TSa. The present BEP model

TABLE III.
Geometrical Parameters of Cyclopropyl Radical (CR), Allyl Radical (AR), Crossing Point (CP), Transition Structure of the BEP Model (TSa), and Transition Structure of Real Potential Energy Surface (TS) for Thermal Ring Opening of Cyclopropyl Radical.

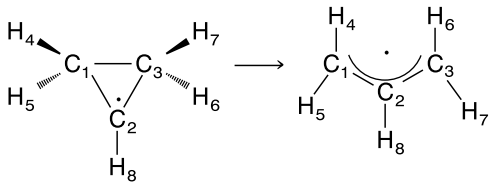

Parameter	CR (C_{2v})	AR (C_{2v})	CP (C_2)	TSa (C_1)	TS (C_1)
C_2C_1	1.454	1.383	1.399	1.407	1.421
C_3C_2	1.454	1.383	1.399	1.423	1.433
H_4C_1	1.106	1.095	1.100	1.084	1.095
H_5C_1	1.106	1.094	1.088	1.081	1.095
H_6C_3	1.106	1.095	1.100	1.087	1.093
H_7C_3	1.106	1.094	1.088	1.084	1.093
H_8C_2	1.064	1.105	1.064	1.065	1.077
$C_3C_2C_1$	63.0	123.7	78.0	85.3	85.5
$H_4C_1C_2$	119.6	121.9	120.4	125.7	121.3
$H_5C_1C_2$	119.6	121.4	123.9	106.1	120.9
$H_6C_3C_2$	119.6	121.9	120.4	118.0	119.9
$H_7C_3C_2$	119.6	121.4	123.9	119.9	121.2
$H_8C_2C_1$	148.5	118.1	141.1	134.2	135.4
$H_4C_1C_2C_3$	108.1	0.0	69.3	265.5	79.4
$H_5C_1C_2C_3$	251.9	180.0	238.8	102.9	249.6
$H_6C_3C_2C_1$	108.1	0.0	69.3	73.6	98.9
$H_7C_3C_2C_1$	251.9	180.0	238.8	243.7	268.6
$H_8C_2C_1C_3$	180.0	180.0	180.0	115.8	158.7

Bond lengths in angstroms and bond and dihedral angles in degrees. Molecular point group symmetry given in parentheses. Note that the hydrogens of the two methylene groups of CR and AR are related through a conrotatory motion.

predicts an activation energy barrier for the ring opening of CR into AR of 23.2 kcal mol^{-1}, whereas the UHF/AM1 activation energy barrier is 24.5 kcal mol^{-1}. Finally, we note that the scalar s at point CP is 0.45, which clearly indicates that the 3B option cannot be applied.

REARRANGEMENT OF *TRANS*-HYDROXYCARBENE TO FORMALDEHYDE

The reaction was studied by several investigators at the *ab initio*[26–28] and semiempirical[29] levels. We now present a study of this reaction using the proposed BEP model options 3A and 3B by using the AM1 Hamiltonian.[25] AM1 predicts an activation energy barrier for the rearrangement of *trans*-hydroxycarbene (tHC) to formaldehyde (F) of 46.1 kcal mol^{-1}. The overall results are shown in Table IV. CP is found to lie 52.3 kcal mol^{-1} above tHC at the AM1 level.

Using the BEP model, option 3A, the converged geometry of the approximate transition state, TSaA, is much closer to the real transition structure of the real AM1 PES, TS, than the geometry of the crossing point, CP. We note that, in this case, RMS (CP − TS) = 0.23, and RMS (TSaA − TS) = 0.13. Diagonalizing the Hessian matrix computed according to eq. (A3-3), it was found that this point is the transition state predicted by the BEP model for this reaction. Also, this model predicts an activation energy barrier with respect to tHC of 47.4 kcal mol^{-1}, which is very close to that predicted by AM1. The resonance energy term, $V_{tHC,F}$, is

TABLE IV.
Geometrical Parameters of *trans*-Hydroxycarbene (tHC), Formaldehyde (F), Crossing Point (CP), Transition Structure of BEP Model Option 3A (TSaA), Transition Structure of BEP Model Option 3B (TSaB), and Transition Structure of Real Potential Energy Surface (TS) for the Rearrangement of *trans*-Hydroxycarbene to Formaldehyde.

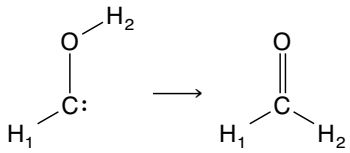

Parameter	tHC (C_s)	F (C_{2v})	CP (C_s)	TSaA (C_s)	TSaB (C_s)	TS (C_s)
H_1C	1.113	1.110	1.066	1.092	1.061	1.096
CO	1.313	1.227	1.243	1.272	1.240	1.291
H_2O	0.975	2.048	1.224	1.257	1.207	1.279
H_1CO	110.0	122.2	134.0	123.1	133.5	122.4
H_2OC	108.3	27.3	58.1	62.6	60.5	61.9
H_2OCH_1	180.0	180.0	180.0	180.0	180.0	180.0

Bond lengths in angstroms and bond and dihedral angles in degrees. Molecular point group symmetry given in parentheses.

-26.0 kcal mol^{-1} and -35.9 kcal mol^{-1} at $\mathbf{q}_{CP}$ and $\mathbf{q}_{TSaA}$, respectively. This represents an increase in the resonance energy term by a factor of 1.4 in passing from CP to TSaA. The contribution weights of the reactant and product in TSaA are $(c_{tHC})^2 = 0.68$ and $(c_F)^2 = 0.32$, respectively, which means that, according to the BEP model, TSaA has a strong contribution of tHC. Because the reaction is highly exothermic, -47.7 kcal mol^{-1}, we conclude that this reaction obeys the Hammond postulate.[5b]

On the other hand, using the BEP model (option 3B), we found a transition state, TSaB, close to the geometry of CP. We note that RMS (TSaB $-$ TS) = 0.22, and RMS (CP $-$ TSaB) = 0.05. The proximity of both geometries, CP and TSaB, is due to the value of the square gradient norm of the function $w_{tHC}V_{tHC,tHC} + w_FV_{F,F}$ at CP is 10.6 kcal/mol Å^{-1}. Diagonalizing the Hessian matrix of TSaB, computed using eq. (A3-3), it was found that this point is the transition state predicted by the proposed BEP model, option 3B. The scalar s, defined in eq. (8), is 0.65, which supports the use of option 3B for this reaction. This BEP model predicts an activation energy barrier of 52.7 kcal mol^{-1} and the weight contributions to TSaB are $(c_{tHC})^2 = 0.66$ and $(c_F)^2 = 0.34$.

Note that the differences among the four points, CP, TSaA, TSaB, and TS, are not large; consequently, in this reaction, the resonance term plays a minor role and practically in the direction of the $N(\mathbf{g}_R - \mathbf{g}_P)$ vector.

REARRANGEMENT OF BICYCLO[3.1.0]HEX-3-EN-2-IL RADICAL TO CYCLOHEXADIENYL RADICAL

This reaction was studied at the *ab initio* level of theory by Olivella and Solé.[30] According to these investigators, the thermal ring opening of the bicyclo[3.1.0]hex-3-en-2-il radical, BCHR, to give the cyclohexadienyl radical, CHR, was calculated to be a symmetry-forbidden electrocyclic process that takes place via the highly unsymmetric transition state lying about 16 kcal mol^{-1} above BCHR. The equilibrium geometry of BCHR has C_s symmetry, whereas CHR has C_{2v} symmetry. The electronic ground state of BCHR is $^2A''$, whereas the CHR is $^2B_1$, which corresponds to a $^2A'$ if we take into account the lower symmetry point group C_s. In other words, BCHR and CHR belong to different symmetry classes of the common point group C_s.[30] It is important to emphasize that the present reaction involves an increasing electronic π-delocalization through the evolution from BCHR to CHR.

We studied this reaction using the proposed BEP model options 3A and 3B within the frame-

work of the UHF method with the split-valence plus *d*-polarization 6-31G* basis set.[31] This level of theory predicts an activation energy barrier for the rearrangement of BCHR to CHR of 23.2 kcal mol^{-1}. The CP point was found to lie 51.5 kcal mol^{-1} above BCHR in the UHF/6-31G* PES. Using the BEP algorithm (option 3A), we located a saddle point in the BEP PES, called TSaA. Diagonalizing the Hessian matrix of TSaA, computed using eq. (A3-3), it was found that this point is the transition state predicted by the proposed BEP model, option 3A. The TSaA is found to lie 35.7 and 47.1 kcal mol^{-1} above BCHR in the UHF/6-31G* PES and the BEP PES, respectively. The contribution weights of the reactant and product in TSaA were $(c_{BCHR})^2 = 0.10$ and $(c_{CHR})^2 = 0.90$, respectively, which means that, according to this BEP model, TSaA has a strong CHR contribution. Because the electronic π-delocalization is much more important in CHR that in BCHR, then, according to the aforementioned weights, TSaA presents a strong electronic π-delocalization. In other words, the resonance effects are very important in this reaction.

Taking the TSaA as the starting geometry to find the real TS, that it is the saddle point on the UHF/6-31G* PES, the NR algorithm needed nine iterations to converge. On the other hand, taking the CP as the starting geometry then the algorithm NR needed 15 iterations to locate the real TS. The optimization was carried out using the GAUSSIAN-94 system of programs.[32] Despite the different number of iterations to reach convergence, both CP and TSaA are equidistant to the real TS. This fact can be noted by looking at the corresponding RMS (RMS [CP − TS] = 8.66, and RMS [TSaA − TS] = 8.73). The geometries of BCHR, CHR, CP, TSaA, and TS are shown in Table V.

Using the BEP model, option 3B, we found a transition state, TSaB, close to the geometry of CP, with RMS (CP − TSaB) = 0.20. Diagonalizing the Hessian matrix of TSaB, computed using eq. (A3-3), it was found that this point is the transition state predicted by the proposed BEP model (option 3B). This BEP model predicted an activation energy barrier of 49.6 kcal mol^{-1}. Taking the TSaB as the starting geometry to locate the real TS, the NR algorithm[32] needed 14 iterations to reach convergence. The RMS between TSaB and TS is 8.61. The scalar, *s*, defined in eq. (8), was 0.68, which supports the use of the option 3B for this reaction.

From these results we conclude that option 3A is better than option 3B and, consequently, option 3A should be used as a standard option. However, in cases in which use of the Hessian matrix is very expensive, one can then use option 3B.

Conclusions

The aim of this article was to show that the BEP model, with the mathematical description given earlier for choosing elements V_{RR}, V_{PP}, and V_{RP}, provides a reasonable approximation to the PES for a variety of elementary reactions of molecules of middle size. For this reason, this BEP model can be used to find approximate TSs in an inexpensive manner. Moreover, it affords the weights of the contributions of reactants and products to the approximate TS in the context of the proposed BEP model.

Acknowledgments

We are indebted to Professor S. Olivella for his valuable suggestions. We acknowledge Professor F. Jensen for a reprint of ref. 11b.

Appendix A1: Partitioning Technique Applied to Secular Equation given by Wave Function of Eq. (5)

The secular equation resulting of the wave function proposed in eq. (5) is:

$$\begin{pmatrix} \langle\Phi_R|H_{ele}|\Phi_R\rangle & \langle\Phi_R|H_{ele}|\Phi_P\rangle & \langle\Phi_R|H_{ele}|\Phi_I\rangle \\ \langle\Phi_P|H_{ele}|\Phi_R\rangle & \langle\Phi_P|H_{ele}|\Phi_P\rangle & \langle\Phi_P|H_{ele}|\Phi_I\rangle \\ \langle\Phi_I|H_{ele}|\Phi_R\rangle & \langle\Phi_I|H_{ele}|\Phi_P\rangle & \langle\Phi_I|H_{ele}|\Phi_I\rangle \end{pmatrix} \times \begin{pmatrix} c_R \\ c_P \\ c_I \end{pmatrix} = V_{adi} \begin{pmatrix} c_R \\ c_P \\ c_I \end{pmatrix} \quad \text{(A1-1)}$$

Following Löwdin,[18] this secular equation can be partitioned as follows:

$$\begin{pmatrix} \langle\Phi_R|H_{ele}|\Phi_R\rangle & \langle\Phi_R|H_{ele}|\Phi_P\rangle \\ \langle\Phi_P|H_{ele}|\Phi_R\rangle & \langle\Phi_P|H_{ele}|\Phi_P\rangle \end{pmatrix} \begin{pmatrix} c_R \\ c_P \end{pmatrix} + \begin{pmatrix} \langle\Phi_R|H_{ele}|\Phi_I\rangle \\ \langle\Phi_P|H_{ele}|\Phi_I\rangle \end{pmatrix} c_I = V_{adi} \begin{pmatrix} c_R \\ c_P \end{pmatrix} \quad \text{(A1-2a)}$$

$$(\langle\Phi_I|H_{ele}|\Phi_R\rangle \quad \langle\Phi_I|H_{ele}|\Phi_P\rangle) \begin{pmatrix} c_R \\ c_P \end{pmatrix} + \langle\Phi_I|H_{ele}|\Phi_I\rangle c_I = V_{adi} c_I \quad \text{(A1-2b)}$$

TABLE V.

Geometrical Parameters of Bicyclo[3.1.0]hex-3-en-2-yl Radical (BCHR), Cyclohexadienyl Radical (CHR), Crossing Point (CP), Transition Structure of BEP Model Option 3A (TSaA), Transition Structure of BEP Model Option 3B (TSaB), and Transition Structure of Real Potential Energy Surface (TS) for Rearrangement of Bicyclo[3.1.0]hex-3-en-2-yl Radical to Cyclohexadienyl Radical.

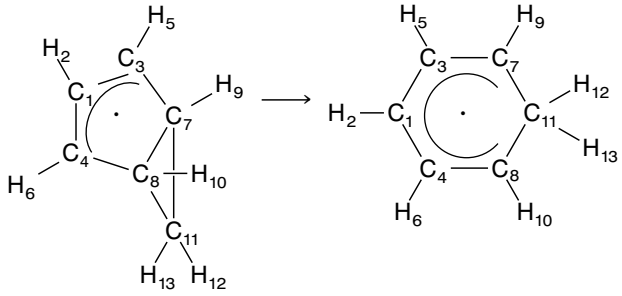

Parameter	BCHR (C_s)	CHR (C_{2v})	CP (C_1)	TSaA (C_1)	TSaB (C_1)	TS (C_1)
C_1H_2	1.074	1.075	1.072	1.073	1.073	1.075
C_1C_3	1.396	1.419	1.397	1.363	1.388	1.371
C_1C_4	1.396	1.419	1.397	1.430	1.398	1.425
C_3H_5	1.073	1.076	1.072	1.074	1.072	1.075
C_4H_6	1.073	1.076	1.073	1.076	1.073	1.076
C_7C_3	1.492	1.373	1.488	1.522	1.496	1.487
C_8C_4	1.492	1.373	1.464	1.433	1.470	1.426
C_7H_9	1.076	1.076	1.085	1.078	1.085	1.073
C_8H_{10}	1.076	1.076	1.085	1.080	1.084	1.076
C_1C_{11}	2.976	2.916	3.321	3.173	3.362	2.909
$C_{11}H_{12}$	1.076	1.092	1.083	1.078	1.083	1.080
$C_{11}H_{13}$	1.076	1.092	1.108	1.098	1.105	1.083
$C_3C_1H_2$	124.8	120.1	124.4	123.3	123.9	123.5
$C_4C_1H_2$	124.8	120.1	125.1	125.1	124.3	123.1
$H_5C_3C_1$	126.1	119.2	124.4	124.2	125.0	124.0
$H_6C_4C_1$	126.1	119.2	123.5	122.3	123.6	122.3
$C_7C_3C_1$	109.5	121.3	116.6	116.7	114.0	114.5
$C_8C_4C_1$	109.5	121.3	117.9	118.9	116.6	115.8
$H_9C_7C_3$	120.0	120.1	113.0	115.2	113.9	122.5
$H_{10}C_8C_4$	120.0	120.1	113.2	115.6	113.4	120.7
$C_{11}C_1C_3$	58.9	59.9	55.9	56.6	51.5	59.4
$H_{12}C_{11}C_1$	165.8	127.7	162.7	157.2	161.3	165.0
$H_{13}C_{11}H_{12}$	114.8	104.6	107.5	108.4	107.7	111.5
$C_4C_1H_2C_3$	178.0	180.0	164.2	169.4	159.4	−176.9
$H_5C_3C_1H_2$	−0.9	0.0	−27.8	−24.9	−28.5	1.8
$H_6C_4C_1H_2$	0.9	0.0	27.7	29.2	28.3	19.8
$C_7C_3C_1H_2$	176.5	180.0	172.6	174.6	177.1	177.3
$C_8C_4C_1H_2$	−176.5	180.0	−172.9	−170.9	187.6	−170.1
$H_9C_7C_3C_1$	143.1	180.0	141.8	136.9	137.2	126.7
$H_{10}C_8C_4C_1$	−143.1	180.0	−141.2	−144.3	−140.5	−149.1
$C_{11}C_1C_3H_2$	−148.5	180.0	−150.6	−153.8	−148.9	−153.2
$H_{12}C_{11}C_1C_3$	−73.5	−90.0	−82.0	−82.9	−82.6	−84.0
$H_{13}C_{11}H_{12}C_1$	180.0	180.0	180.1	179.3	184.6	174.9

Bond lengths in angstroms and bond and dihedral angles in degrees. Molecular point group symmetry given in parentheses.

From eq. (A1-2b) we get

$$c_I = -(\langle\Phi_I|H_{ele}|\Phi_I\rangle - V_{adi})^{-1} \times(\langle\Phi_I|H_{ele}|\Phi_R\rangle \quad \langle\Phi_I|H_{ele}|\Phi_P\rangle)\begin{pmatrix} c_R \\ c_P \end{pmatrix} \quad \text{(A1-3)}$$

Substituting c_I from eq. (A1-3) in eq. (A1-2a) we obtain:

$$\left[\begin{pmatrix} \langle\Phi_R|H_{ele}|\Phi_R\rangle & \langle\Phi_R|H_{ele}|\Phi_P\rangle \\ \langle\Phi_P|H_{ele}|\Phi_R\rangle & \langle\Phi_P|H_{ele}|\Phi_P\rangle \end{pmatrix} - \begin{pmatrix} \langle\Phi_R|H_{ele}|\Phi_I\rangle \\ \langle\Phi_P|H_{ele}|\Phi_I\rangle \end{pmatrix}(\langle\Phi_I|H_{ele}|\Phi_I\rangle - V_{adi})^{-1} \times(\langle\Phi_I|H_{ele}|\Phi_R\rangle \quad \langle\Phi_I|H_{ele}|\Phi_P\rangle)\right]\begin{bmatrix} c_R \\ c_P \end{bmatrix} = V_{adi}\begin{bmatrix} c_R \\ c_P \end{bmatrix} \quad \text{(A1-4)}$$

Finally, rearranging eq. (A1-4) and using the definitions given in eqs. (A1-6) we get:

$$\begin{pmatrix} \langle\Phi_R|H_{ele}|\Phi_R\rangle - \langle\Phi_R|H_{ele}|\Phi_I\rangle(\langle\Phi_I|H_{ele}|\Phi_I\rangle - V_{adi})^{-1}\langle\Phi_I|H_{ele}|\Phi_R\rangle & \langle\Phi_R|H_{ele}|\Phi_P\rangle - \langle\Phi_R|H_{ele}|\Phi_I\rangle(\langle\Phi_I|H_{ele}|\Phi_I\rangle - V_{adi})^{-1}\langle\Phi_I|H_{ele}|\Phi_P\rangle \\ \langle\Phi_P|H_{ele}|\Phi_R\rangle - \langle\Phi_P|H_{ele}|\Phi_I\rangle(\langle\Phi_I|H_{ele}|\Phi_I\rangle - V_{adi})^{-1}\langle\Phi_I|H_{ele}|\Phi_R\rangle & \langle\Phi_P|H_{ele}|\Phi_P\rangle - \langle\Phi_P|H_{ele}|\Phi_I\rangle(\langle\Phi_I|H_{ele}|\Phi_I\rangle - V_{adi})^{-1}\langle\Phi_I|H_{ele}|\Phi_P\rangle \end{pmatrix}\begin{pmatrix} c_R \\ c_P \end{pmatrix} = \begin{pmatrix} V_{RR} & V_{RP} \\ V_{PR} & V_{PP} \end{pmatrix}\begin{pmatrix} c_R \\ c_P \end{pmatrix} = V_{adi}\begin{pmatrix} c_R \\ c_P \end{pmatrix} \quad \text{(A1-5)}$$

Eq. (A1-5) can be seen as the 2×2 secular equation form of the 3×3 secular eq. (A1-1). From eq. (A1-5) we see that the elements, V_{RR}, V_{PP}, and V_{RP}, are:

$$V_{RR} = \langle\Phi_R|H_{ele}|\Phi_R\rangle - \langle\Phi_R|H_{ele}|\Phi_I\rangle \times(\langle\Phi_I|H_{ele}|\Phi_I\rangle - V_{adi})^{-1}\langle\Phi_I|H_{ele}|\Phi_R\rangle \quad \text{(A1-6a)}$$

$$V_{PP} = \langle\Phi_P|H_{ele}|\Phi_P\rangle - \langle\Phi_P|H_{ele}|\Phi_I\rangle \times(\langle\Phi_I|H_{ele}|\Phi_I\rangle - V_{adi})^{-1}\langle\Phi_I|H_{ele}|\Phi_P\rangle \quad \text{(A1-6b)}$$

$$V_{RP} = V_{PR} = \langle\Phi_R|H_{ele}|\Phi_P\rangle - \langle\Phi_R|H_{ele}|\Phi_I\rangle \times(\langle\Phi_I|H_{ele}|\Phi_I\rangle - V_{adi})^{-1}\langle\Phi_I|H_{ele}|\Phi_P\rangle \quad \text{(A1-6c)}$$

Appendix A2: Deduction of Chang–Miller Formula to Evaluate Element V_{RP}

Here, we summarize only the expressions obtained by Chang and Miller[19] to evaluate the resonance integral, V_{RP}, used in the present work. First, eq. (4) can be rearranged as follows:

$$V_{RP}^2 = (V_{RR} - V_{adi})(V_{PP} - V_{adi}) \quad \text{(A2-1)}$$

We expand the BEP adiabatic potential, V_{adi}, around a selected point $\mathbf{q}_0$ to second order:

$$V_{adi} = V_{adi}^0 + (\mathbf{g}_{adi}^0)^T\Delta\mathbf{q}_0 + \tfrac{1}{2}\Delta\mathbf{q}_0^T\mathbf{H}_{adi}^0\Delta\mathbf{q}_0 \quad \text{(A2-2)}$$

where $\Delta\mathbf{q}_0 = \mathbf{q} - \mathbf{q}_0$, $\mathbf{g}_{adi}^0$ is the gradient vector and $\mathbf{H}_{adi}^0$ the Hessian matrix of V_{adi} at point $\mathbf{q}_0$. It is assumed that the quadratic expansion around $\mathbf{q}_0$ given in eq. (A2-2), $\mathbf{H}_{adi}^0 = \mathbf{H}_{TS}$, is the Hessian matrix of the real PES at $\mathbf{q}_{TS}$. In other words, $\mathbf{q}_{TS}$ is the stationary point of the quadratic eq. (A2-2). On the other hand, potentials V_{RR} and V_{PP} are also expanded quadratically around point $\mathbf{q}_0$, namely:

$$V_{ii} = V_{ii}^0 + (\mathbf{g}_i^0)^T\Delta\mathbf{q}_0 + \tfrac{1}{2}\Delta\mathbf{q}_0^T\mathbf{H}_i\Delta\mathbf{q}_0 \quad \text{(A2-3)}$$

where $\mathbf{g}_i^0$ is the gradient vector of V_{ii} at point $\mathbf{q}_0$, given by:

$$\mathbf{g}_i^0 = \mathbf{H}_i(\mathbf{q}_0 - \mathbf{q}_i) \quad \text{(A2-4)}$$

and:

$$V_{ii}^0 = V_{ii}^* + \tfrac{1}{2}(\mathbf{q}_0 - \mathbf{q}_i)^T\mathbf{H}_i(\mathbf{q}_0 - \mathbf{q}_i) \quad \text{(A2-5)}$$

for $i = R, P$. In eqs. (A2-4) and (A2-5), vector $\mathbf{q}_i$ corresponds to the equilibrium geometry, V_{ii}^* to its energy, and $\mathbf{H}_i$ to the corresponding force constant matrix. Note that both $\mathbf{H}_i$ matrices are positive definite. Now, substituting eqs. (A2-2) and (A2-3) in eq. (A2-1) we get an expansion expression for V_{RP}^2 to second order in $\Delta\mathbf{q}_0$, namely:

$$\begin{aligned} V_{RP}^2 = {} & (V_{RR}^0 - V_{adi}^0)(V_{PP}^0 - V_{adi}^0) \\ & + \Delta\mathbf{q}_0^T\big[(V_{RR}^0 - V_{adi}^0)(\mathbf{g}_P^0 - \mathbf{g}_{adi}^0) \\ & + (V_{PP}^0 - V_{adi}^0)(\mathbf{g}_R^0 - \mathbf{g}_{adi}^0)\big] \\ & + \tfrac{1}{2}\Delta\mathbf{q}_0^T\Big[(V_{RR}^0 - V_{adi}^0)(\mathbf{H}_P - \mathbf{H}_{adi}^0) \\ & + (V_{PP}^0 - V_{adi}^0)(\mathbf{H}_R - \mathbf{H}_{adi}^0) \\ & + (\mathbf{g}_P^0 - \mathbf{g}_{adi}^0)(\mathbf{g}_R^0 - \mathbf{g}_{adi}^0)^T \\ & + (\mathbf{g}_R^0 - \mathbf{g}_{adi}^0)(\mathbf{g}_P^0 - \mathbf{g}_{adi}^0)^T\Big]\Delta\mathbf{q}_0 \end{aligned} \quad \text{(A2-6)}$$

Following Chang and Miller[19] instead of eq. (A2-6) we use a cumulant resummation, because it gives better extrapolation. Consequently, V_{RP}^2 is taken as a generalized Gaussian:

$$V_{RP}^2 = A_0 \exp\left(\mathbf{b}_0^T\Delta\mathbf{q}_0 + \tfrac{1}{2}\Delta\mathbf{q}_0^T\mathbf{B}_0\Delta\mathbf{q}_0\right) \quad \text{(A2-7)}$$

where:

$$A_0 = (V_{RR}^0 - V_{adi}^0)(V_{PP}^0 - V_{adi}^0) \quad \text{(A2-8)}$$

$$\begin{aligned} \mathbf{b}_0 = {} & \frac{1}{V_{RR}^0 - V_{adi}^0}(\mathbf{g}_R^0 - \mathbf{g}_{adi}^0) \\ & + \frac{1}{V_{PP}^0 - V_{adi}^0}(\mathbf{g}_P^0 - \mathbf{g}_{adi}^0) \end{aligned} \quad \text{(A2-9)}$$

$$\begin{aligned} \mathbf{B}_0 = {} & \frac{1}{V_{RR}^0 - V_{adi}^0}(\mathbf{H}_R - \mathbf{H}_{adi}^0) \\ & + \frac{1}{V_{PP}^0 - V_{adi}^0}(\mathbf{H}_P - \mathbf{H}_{adi}^0) \\ & - \frac{1}{(V_{RR}^0 - V_{adi}^0)^2}(\mathbf{g}_R^0 - \mathbf{g}_{adi}^0)(\mathbf{g}_R^0 - \mathbf{g}_{adi}^0)^T \\ & - \frac{1}{(V_{PP}^0 - V_{adi}^0)^2}(\mathbf{g}_P^0 - \mathbf{g}_{adi}^0)(\mathbf{g}_P^0 - \mathbf{g}_{adi}^0)^T \end{aligned} \quad \text{(A2-10)}$$

Eqs. (A2-7)–(A2-10), along with (A2-5) and (4), are the basic expressions used to compute the BEP adiabatic PES, V_{adi}.

Appendix A3: Gradient and Hessian of V_{adi} Evaluated Using Eqs. (4), (A2-5), and (A2-7) with Respect to Internal Coordinates

Differentiating eq. (4) with respect to internal coordinates, $\mathbf{q}$, and using the two eqs. (A2-5), we obtain the gradient vector of the BEP adiabatic PES, V_{adi}:

$$\begin{aligned} \nabla_{\mathbf{q}} V_{adi} = {} & \mathbf{g}_{adi} \\ = {} & \frac{\mathbf{g}_R + \mathbf{g}_P}{2} - \left[\left(\frac{V_{RR} - V_{PP}}{2}\right)^2 + V_{RP}^2\right]^{-1/2} \\ & \times\left[\left(\frac{V_{RR} - V_{PP}}{2}\right)\left(\frac{\mathbf{g}_R - \mathbf{g}_P}{2}\right) + \frac{1}{2}\mathbf{g}_{RP}\right] \end{aligned} \quad \text{(A3-1)}$$

where:

$$\mathbf{g}_{RP} = V_{RP}^2(\mathbf{b}_0 + \mathbf{B}_0\Delta\mathbf{q}_0) \quad \text{(A3-2)}$$

is the gradient vector of V_{RP}^2 evaluated according to eq. (A2-7) and $\mathbf{g}_i$ is the gradient vector of the quadratic PES V_{ii}, given in eqs. (A2-4), at the point $\mathbf{q}$ for $i = R, P$. Differentiating eq. (A3-1) with respect to the internal coordinates, $\mathbf{q}$, we obtain the Hessian matrix of V_{adi}:

$$\begin{aligned} \nabla_{\mathbf{q}}\nabla_{\mathbf{q}}^T V_{adi} = {} & \mathbf{H}_{adi} \\ = {} & \frac{\mathbf{H}_R + \mathbf{H}_P}{2} + \left[\left(\frac{V_{RR} - V_{PP}}{2}\right)^2 + V_{RP}^2\right]^{-3/2} \\ & \times\left[\left(\frac{V_{RR} - V_{PP}}{2}\right)\left(\frac{\mathbf{g}_R - \mathbf{g}_P}{2}\right) + \frac{1}{2}\mathbf{g}_{RP}\right] \\ & \times\left[\left(\frac{V_{RR} - V_{PP}}{2}\right)\left(\frac{\mathbf{g}_R - \mathbf{g}_P}{2}\right) + \frac{1}{2}\mathbf{g}_{RP}\right]^T \\ & - \left[\left(\frac{V_{RR} - V_{PP}}{2}\right)^2 + V_{RP}^2\right]^{-1/2} \\ & \times\left[\left(\frac{V_{RR} - V_{PP}}{2}\right)\left(\frac{\mathbf{H}_R - \mathbf{H}_P}{2}\right)\right. \\ & \left. + \left(\frac{\mathbf{g}_R - \mathbf{g}_P}{2}\right)\left(\frac{\mathbf{g}_R - \mathbf{g}_P}{2}\right)^T + \frac{1}{2}\mathbf{H}_{RP}\right] \end{aligned} \quad \text{(A3-3)}$$

where:

$$\mathbf{H}_{RP} = V_{RP}^2\left[\mathbf{B}_0 + (\mathbf{b}_0 + \mathbf{B}_0\Delta\mathbf{q}_0)(\mathbf{b}_0 + \mathbf{B}_0\Delta\mathbf{q}_0)^T\right] \tag{A3-4}$$

is the Hessian matrix of V_{RP}^2 evaluated according to eq. (A2-7). These expressions are a specific case of those given in ref. 20.

Appendix A4: Proof of Domain of Lagrangian Multiplier of Eq. (1)

The extrema of eq. (1) can be obtained as solution of the equation set:

$$\nabla_{\mathbf{q}} L(\mathbf{q}, \lambda) = w_R\mathbf{g}_R + w_P\mathbf{g}_P + \lambda(\mathbf{g}_R - \mathbf{g}_P) = 0 \tag{A4-1}$$

and eq. (1b), where $\mathbf{g}_i$ is the gradient vector of V_{ii} at point $\mathbf{q}$ for $i = R, P$. The definition of V_{ii} is that given in equation (A2-5). From eq. (A4-1), one finds that:

$$\mathbf{g}_R = \left(\frac{\lambda - w_P}{\lambda + w_P}\right)\mathbf{g}_P = \xi\mathbf{g}_P \tag{A4-2}$$

Because the crossing point should be near the TS, then, according to Ruedenberg and Sun,[12] the two gradients $\mathbf{g}_R$ and $\mathbf{g}_P$ should be antiparallels; that is, $\xi < 0$. Using this constraint and the fact that $w_R + w_P = 1$, we can find the domain of the Lagrangian multiplier λ:

$$\xi = \frac{\lambda - w_P}{\lambda + w_R} = \frac{\lambda + w_R - 1}{\lambda + w_R} = 1 - \frac{1}{\lambda + w_R} < 0 \tag{A4-3}$$

From eq. (A4-3) we conclude that $0 < \lambda + w_R < 1$, or similarly, $-w_R < \lambda < w_P$. Taking $w_R = w_P = 1/2$ and multiplying the inequality by 2, we obtain the results of Ruedenberg and Sun.[12] Finally, we note that parameter ξ can be transformed into a useful reaction coordinate parameter, rc, with domain 0 (in reactants) $< rc < 1$ (in products). According to Ruedenberg and Sun,[12] $\xi = 0$ at $\mathbf{q}_R$ and $\xi = -\infty$ at $\mathbf{q}_P$. With these considerations we define the function:

$$rc = \frac{\xi}{\xi - 1} \tag{A4-4}$$

We observe that:

$$\lim_{\xi \to -0} rc = 0 \tag{A4-5a}$$

and:

$$\lim_{\xi \to -\infty} rc = 1 \tag{A4-5b}$$

Appendix A5: Müller–Brown Two-Dimensional Potential Energy Surface

The mathematical expression and parameters used to define de Müller–Brown PES are[22]:

$$V(x, y) = \mathbf{a}^T\mathbf{f}(x, y) \tag{A5-1}$$

where:

$$\mathbf{a}^T = (-200 \quad -100 \quad -170 \quad 15)$$

$$\mathbf{f}^T(x, y) = (f_1(x, y) \quad f_2(x, y) \quad f_3(x, y) \quad f_4(x, y))$$

and each $f_i(x, y)$ is defined as:

$$f_i(x, y) = \exp\left(\frac{1}{2}\Delta\mathbf{q}_i^T\mathbf{F}_i\Delta\mathbf{q}_i\right) \qquad \forall i = 1, 4 \tag{A5-2}$$

In eq. (A5-2), $\Delta\mathbf{q}_i = \mathbf{q} - \mathbf{q}_i^0$, $\mathbf{q}^T = (x \; y)$ and $(\mathbf{q}_i^0)^T = (x_i^0 \; y_i^0)$. The set of symmetric square matrices $\{\mathbf{F}_i\}_{i=1}^4$ that appear in eq. (A5-2) are taken as:

$$\mathbf{F}_1 = \begin{pmatrix} -2 & 0 \\ 0 & -20 \end{pmatrix} \qquad \mathbf{F}_2 = \begin{pmatrix} -2 & 0 \\ 0 & -20 \end{pmatrix}$$

$$\mathbf{F}_3 = \begin{pmatrix} -13 & 11 \\ 11 & -13 \end{pmatrix} \qquad \mathbf{F}_4 = \begin{pmatrix} 1.4 & 0.6 \\ 0.6 & 1.4 \end{pmatrix}$$

and the set of the vectors $\{\mathbf{q}_i^0\}_{i=1}^4$ as

$$\mathbf{q}_1^0 = \begin{pmatrix} x_1^0 \\ y_1^0 \end{pmatrix} = \begin{pmatrix} 1 \\ 0 \end{pmatrix} \qquad \mathbf{q}_2^0 = \begin{pmatrix} x_2^0 \\ y_2^0 \end{pmatrix} = \begin{pmatrix} 0 \\ 0.5 \end{pmatrix}$$

$$\mathbf{q}_3^0 = \begin{pmatrix} x_3^0 \\ y_3^0 \end{pmatrix} = \begin{pmatrix} -0.5 \\ 1.5 \end{pmatrix} \qquad \mathbf{q}_4^0 = \begin{pmatrix} x_4^0 \\ y_4^0 \end{pmatrix} = \begin{pmatrix} -1 \\ 1 \end{pmatrix}$$

References

1. (a) Truhlar, D. G.; Garret, B. C.; Klippenstein, S. J. J Phys Chem 1996, 100, 12771; (b) Garret, B. C.; Truhlar, D. G. In: Schleyer, P. v. R., Schaefer III, H. F., eds. Encyclopedia of Computational Chemistry; Wiley: Chichester, UK, 1998.
2. (a) Schlegel, H. B. Adv Chem Phys 1987, 67, 249; (b) Schlegel, H. B. In: Yarkony, D. R., ed. Modern Electronic Structure Theory; World Scientific: Singapore, 1995.
3. Shaik, S.; Ioffe, A.; Reddy, A. C.; Pross, A. J Am Chem Soc 1994, 116, 262.
4. (a) Bell, R. P. Proc R Soc London Ser A 1936, 154, 414; (b) Bell, R. P.; Lidwell, O. M. Proc R Soc London Ser A 1940, 176, 114; (c) Ogg, R. A., Jr.; Polanyi, M. Trans Faraday Soc 1935, 31, 604; (d) Evans, M. G.; Polanyi, M. Trans Faraday Soc 1935, 31, 875; (e) Evans, M. G.; Polanyi, M. Trans Faraday Soc 1936, 32, 1333; (f) Evans, M. G.; Polanyi, M. Trans Faraday Soc 1937, 33, 448; (g) Evans, M. G.; Polanyi, M. Trans Faraday Soc 1938, 34, 11; (h) Evans, M. G.; Warhurst, E. Trans Faraday Soc 1938, 34, 614; (i) Evans, M. G. Trans Faraday Soc 1939, 35, 824. (j) Baughan, E. C.; Evans, M. G.; Polanyi, M. Trans Faraday Soc 1941, 37, 377; (k) Baughan, E. C.; Polanyi, M. Trans Faraday Soc 1941, 37, 648; (l) Evans, M. G. Trans Faraday Soc 1946, 42, 719; (m) Warhurst, E. Trans Faraday Soc 1949, 45, 461; (n) Warhurst, E. Proc R Soc London Ser A 1951, 207, 32.
5. (a) Leffler, J. E. Science 1953, 117, 340; (b) Hammond, G. S. J Am Chem Soc 1955, 77, 334; (c) Thornton, E. R. J Am Chem Soc 1967, 89, 2915; (d) Marcus, R. A. J Phys Chem 1968, 72, 891; (e) More O'Ferrall, R. A. J Chem Soc B 1970, 274; (f) Dewar, M. J. S. J Am Chem Soc 1984, 106, 209.
6. Jencks, W. P. Chem Rev 1985, 85, 511.
7. Salem, L. Electrons in Chemical Reactions: First Principles; Wiley: New York, 1982.
8. (a) Bernardi, F.; Robb, M. A.; Schlegel, H. B.; Tonachini, G. J Am Chem Soc 1984, 106, 1198; (b) Bernardi, F.; Olivucci, M.; Robb, M. A.; Tonachini, G. J Am Chem Soc 1986, 108, 1408; (c) Bernardi, F.; Olivucci, M.; McDouall, J. J. W.; Robb, M. A. J Am Chem Soc 1987, 109, 544; (d) Bernardi, F.; Robb, M. A. Adv Chem Phys 1987, 67, 155.
9. (a) McDouall, J. J. W.; Robb, M. A.; Bernardi, F. Chem Phys Lett 1986, 129, 595; (b) Bernardi, F.; McDouall, J. J. W.; Robb, M. A. J Comput Chem 1987, 8, 296.
10. (a) Morokuma, K.; Koga, N. Chem Phys Lett 1985, 119, 371; (b) Kamiya, K.; Morokuma, K. Chem Phys Lett 1986, 123, 331.
11. (a) Jensen, F. J Am Chem Soc 1992, 114, 1596; (b) Jensen, F. J Comput Chem 1994, 15, 1199.
12. Ruedenberg, K.; Sun, J.-Q. J Chem Phys 1994, 101, 2168.
13. (a) Pross, A.; Shaik, S. S. Tetrahedron Lett 1982, 23, 5467; (b) Pross, A.; Shaik, S. S. Acc Chem Res 1983, 16, 363; (c) Shaik, S. S. Prog Phys Org Chem 1985, 15, 197; (d) Pross, A. Adv Org Chem 1985, 21, 99; (e) Shaik, S. S. Pure Appl Chem 1991, 63, 193; (f) Shaik, S. S.; Schlegel, H. B.; Wolfe, S. Theoretical Aspects of Physical Organic Chemistry. The S_N2 Mechanism; Wiley: New York, 1992.
14. (a) Sini, G.; Shaik, S. S.; LeFour, J.-M.; Ohanessian, G.; Hiberty, P. C. J Phys Chem 1989, 93, 5661; (b) Maitre, P.; Hiberty, P. C.; Ohanessian, G.; Shaik, S. S. J Phys Chem 1990, 94, 4089.
15. (a) Warshel, A.; Weiss, R. M. J Am Chem Soc 1980, 102, 6218; (b) Warshel, A. Biochemistry 1981, 20, 3167; (c) Warshel, A. Acc Chem Res 1981, 14, 284; (d) Hwang, J.-K.; King, G.; Creighton, S.; Warshel, A. J Am Chem Soc 1988, 110, 5297; (e) Aqvist, J.; Warshel, A. Biochemistry 1989, 28, 4680; (f) Warshel, A. Computer Modeling of Chemical Reactions in Enzymes and Solutions; Wiley: New York, 1991; (g) Aqvist, J.; Warshel, A. Chem Rev 1993, 93, 2523.
16. Kim, H. J.; Hynes, J. T. J Am Chem Soc 1992, 114, 10508.
17. (a) Bofill, J. M. J Comput Chem 1994, 15, 1; (b) Bofill, J. M.; Comajuan, M. J Comput Chem 1995, 16, 1326; (c) Bofill, J. M. Chem Phys. Lett 1996, 260, 359.
18. (a) Löwdin, P.-O. J Math Phys 1962, 3, 969; (b) Löwdin, P.-O. J Math Phys 1962, 3, 1171.
19. Chang, Y.-T.; Miller, W. H. J Phys Chem 1990, 94, 5884.
20. Minichino, C.; Voth, G. A. J Phys Chem B 1997, 101, 4544.
21. (a) Cerjan, C. J.; Miller, W. H. J Chem Phys 1981, 75, 2800; (b) Simons, J.; Jørgensen, P.; Taylor, H.; Ozment, J. J Phys Chem 1983, 87, 2745; (c) O'Neal, D.; Taylor, H.; Simons, J. J Phys Chem 1984, 88, 1510; (d) Banerjee, A.; Adams, N.; Simons, J.; Shepard, R. J Phys Chem 1985, 89, 52; (e) Taylor, H.; Simons, J. J Phys. Chem 1985, 89, 684; (f) Baker, J. J Comput Chem 1986, 7, 385; (g) Nichols, J.; Taylor, H.; Schmidt, P.; Simons, J. J Chem Phys 1990, 92, 340; (h) Helgaker, T. Chem Phys Lett 1991, 182, 503; (i) Culot, P.; Dive, G.; Nguyen, V. H.; Ghuysen, J. M. Theor Chim Acta 1992, 82, 189; (j) Anglada, J. M.; Bofill, J. M. Int J Quantum Chem 1997, 62, 153; (k) Besalú, E.; Bofill, J. M. Theor Chem Acc 1998, 100, 265.
22. Müller, K.; Brown, L. D. Theor Chim Acta 1979, 53, 75.
23. Wolfram, S. Mathematica; Addison-Wesley: Redwood City, CA, 1988, and associated computer programs.
24. (a) Olivella, S.; Solé, A.; Bofill, J. M. J Am Chem Soc 1990, 112, 2160; (b) Anglada, J. M.; Bofill, J. M. Chem Phys Lett 1997, 269, 469.
25. Dewar, M. J. S.; Zoebisch, E. G.; Healy, E. F.; Stewart, J. J. P. J Am Chem Soc 1985, 107, 3902.
26. Goddard, J. D.; Schaefer, H. F., III. J Chem Phys 1979, 70, 5117.
27. Lucchese, B. R.; Schaefer, H. F., III. J Am Chem Soc 1978, 100, 298.
28. Harding, L. B.; Schlegel, H. B.; Krishnan, R.; Pople, J. A. J Phys Chem 1980, 84, 3394.
29. Schröder, S.; Thiel, W. J Am Chem Soc 1985, 107, 4422.
30. Olivella, S.; Solé, A. J Am Chem Soc 1991, 113, 8628.
31. Hariharan, P. C.; Pople, J. A. Theor Chim Acta 1973, 28, 213.
32. Frisch, M. J.; Trucks, G. W.; Schlegel, H. B.; Gill, P. M. W.; Johnson, B. G.; Robb, M. A.; Cheeseman, J. R.; Keith, T.; Petersson, G. A.; Montgomery, J. A.; Raghavachari, K.; Al-Laham, M. A.; Zakrzewski, V. G.; Ortiz, J. V.; Foresman, J. B.; Cioslowski, J.; Stefanov, B. B.; Nanayakkara, A.; Challacombe, M.; Peng, C. Y.; Ayala, P. Y.; Chen, W.; Wong, M. W.; Andres, J. L.; Replogle, E. S.; Gomperts, R.; Martin, R. L.; Fox, D. J.; Binkley, J. S.; Defrees, D. J.; Baker, J.; Stewart, J. P.; Head-Gordon, M.; Gonzalez, C.; Pople, J. A. GAUSSIAN; Gaussian, Inc.: Pittsburgh, PA, 1995.